TISSUE ENGINEERING: Part A
Volume 22, Numbers 5 and 6, 2016

DOI: 10.1089/ten.tea.2015.0409

termis
Tissue Engineering
& Regenerative Medicine
International Society

ORIGINAL ARTICLE

Blended Polyurethane and Tropoelastin as a Novel Class of Biologically Interactive Elastomer

Steven G. Wise, PhD,[1–3] Hongjuan Liu, BS,[2,4–6] Giselle C. Yeo, PhD,[3,5] Praveesuda L. Michael, MEng,[1,2] Alex H.P. Chan, BS,[1,2] Alan K.Y. Ngo, BS,[3] Marcela M.M. Bilek, PhD, MBA,[7] Shisan Bao, MD, PhD,[2,4–6] and Anthony S. Weiss, PhD[3,5,6]

Polyurethanes are versatile elastomers but suffer from biological limitations such as poor control over cell attachment and the associated disadvantages of increased fibrosis. We address this problem by presenting a novel strategy that retains elasticity while modulating biological performance. We describe a new biomaterial that comprises a blend of synthetic and natural elastomers: the biostable polyurethane Elast-Eon and the recombinant human tropoelastin protein. We demonstrate that the hybrid constructs yield a class of coblended elastomers with unique physical properties. Hybrid constructs displayed higher elasticity and linear stress–strain responses over more than threefold strain. The hybrid materials showed increased overall porosity and swelling in comparison to polyurethane alone, facilitating enhanced cellular interactions. *In vitro,* human dermal fibroblasts showed enhanced proliferation, while *in vivo,* following subcutaneous implantation in mice, hybrid scaffolds displayed a reduced fibrotic response and tunable degradation rate. To our knowledge, this is the first example of a blend of synthetic and natural elastomers and is a promising approach for generating tailored bioactive scaffolds for tissue repair.

Introduction

Polyurethane elastomers are useful polymers because they exhibit good hemocompatibility and have excellent mechanical performance,[1] which can be tuned by adjusting the ratios and types of precursors, including diisocyanate, macrodiol, and chain extender, to provide a range of formulations and properties.[2] However, the wider use of polyurethane biomaterials has been tempered by concerns over biological tolerance and byproduct toxicity, including their long-term stability following implantation.[3] Changes to the common building blocks of polyurethanes, such as the introduction of polyether linkages, successfully increase resistance to hydrolysis, but raise their susceptibility to oxidative breakdown.[4]

Improved formulations of polyurethanes such as Elast-Eon have been developed to address the problem of long-term biostability[5]; Elast-Eon is synthesized using polyhexamethylene oxide and polydimethylsiloxane, resulting in a soft flexible polyurethane. The long-term biostability of Elast-Eon has been well demonstrated in ovine subcutaneous implant studies for up to 6 months,[6] which reflects the resistance to biological degradation of both polydimethylsiloxane and its well-formed hard blocks.[7] Elast-Eon is used as a long-term implantable material for cardiovascular applications such as replacement grafts, components of blood pumps, stent coatings, catheters, and orthopedic implants.[8] However, it is inherently incapable of modulating the interactions of cells, including fibroblasts, and, as a consequence, promotes an elevated *in vivo* fibrotic response that limits its use in tissue repair.[9]

A useful approach to improve the biological interaction of synthetic polymers has been to blend them with natural materials.[10] Degradable polymer scaffolds such as poly(lactic-co-glycolic acid) (PLGA) and polycaprolactone (PCL) have enhanced bioactivity in blends with collagen for diverse biomedical applications, including improved angiogenesis,[11] nerve guidance,[12] and bladder regeneration.[13] Similarly, polyurethane blends with collagen have shown potential application for vascular regeneration[14] and grafting,[15] while gelatin containing scaffolds have been proposed for wound

[1]The Heart Research Institute, Sydney, Australia.
[2]Sydney Medical School, University of Sydney, Sydney, Australia.
[3]School of Molecular Bioscience, University of Sydney, Sydney, Australia.
[4]Discipline of Pathology and School of Medical Science, University of Sydney, Sydney, Australia.
[5]Charles Perkins Centre, University of Sydney, Sydney, Australia.
[6]Bosch Institute, University of Sydney, Sydney, Australia.
[7]School of Physics, University of Sydney, Sydney, Australia.

repair.[16] Multicomponent systems, which include elastin, collagen, and polyurethane, have also been studied in an effort to balance mechanical and biocompatibility considerations.[17]

Human tropoelastin is the precursor of the natural human elastomer elastin and is secreted from a number of cell types, including smooth muscle cells, fibroblasts, and endothelial cells.[18] Tropoelastin is known to interact with the surrounding cell types, affecting chemotaxis, morphogenesis, proliferation, ion transport, and actin fiber formation through well-characterized binding receptors, including the elastin binding proteins, integrins, and glycosaminoglycans.[19] Electrospun tropoelastin modulates the attachment, spreading, and proliferation of multiple cell types, including primary dermal fibroblasts,[20] endothelial cells, and coronary artery smooth muscle cells.[21] Incorporated in scaffolds, human tropoelastin promotes cell proliferation[22] and blends with the relatively stiff PLGA[23] and PCL to confer enhanced growth of endothelial cells, increased elasticity, and improved blood compatibility,[24] while tropoelastin/collagen hybrids show significantly improved performance for dermal scaffolding applications.[25]

We reasoned that a coblend of polyurethane Elast-Eon E2A (denoted as E2A) and tropoelastin would uniquely result in a scaffold combining strength, elasticity, and cell interactivity. In this study, we present a new class of elastic hybrids comprising blended E2A polyurethane and recombinant human tropoelastin, with enhanced elasticity and fibroblast interactions over E2A alone. We further demonstrate a reduced fibrotic response and the opportunity to modulate cell infiltration and scaffold degradation *in vivo* by fine-tuning the electrospinning flow rate used during hybrid production.

Materials and Methods

Reagents

Recombinant human tropoelastin (tropoelastin) corresponding to amino acid residues 27-724 of GenBank entry AAC98394 (gi 182020) was expressed and purified as previously described.[26] E2A (MW ≥95,000 g/mol) beads were provided by AorTech Biomaterials and incorporated hard segments of 4,4-methylenediphenyl diisocyanate and 1,4-butanediol, and a mixed soft segment of PDMS and poly (hexamethylene oxide) in the ratio of 80:20.[9] Human dermal fibroblasts (HDF; line GM3348) were obtained from Coriell Research Institute (Camden, NJ) and used up to passage 14. Other reagents were purchased from Sigma-Aldrich unless otherwise stated.

Electrospinning

Solutions dissolved in 1,1,1,3,3,3-hexafluro-2-propanol were electrospun by loading into a syringe equipped with a blunt 18G needle. E2A was prepared in concentrations ranging from 5% to 10% w/v. Tropoelastin-only scaffolds were prepared from 20% w/v solutions, as previously described.[20] Hybrid materials were optimally electrospun from 1 mL solution containing 100 mg E2A and 200 mg tropoelastin. Constant flow rates (1, 3, or 5 mL/h) were achieved using a syringe pump and the needle connected to the positive output of a high-voltage power supply. Fibers were electrospun onto a flat metal target to produce rectangular sheets.[24] Dry scaffolds were placed in an open stage desiccator and crosslinked by vapor from a separate 25% (v/v) aqueous glutaraldehyde (GA) solution. Unreacted GA in the scaffolds was quenched by 0.2 M glycine solution overnight. Scaffolds were then washed repeatedly in phosphate-buffered saline (PBS).[25] More than half of the 35 free lysines on each tropoelastin molecule react with GA within 2 h, with the optimal balance between crosslinking and scaffold rehydration achieved between 8 and 16 h where scaffolds are composed entirely of tropoelastin.[21]

Scanning electron microscopy/fiber quantification

Samples for scanning electron microscopy (SEM) analysis were fixed in 2.5% GA in 0.1 M sodium phosphate buffer (PB), postfixed with 1% (v/v) osmium tetraoxide in 0.1 M PB, and dehydrated in ascending grades of ethanol before drying with hexamethyldisilasane. The samples were sputter coated with 20 nm gold and imaged with a Zeiss EVO 50 scanning electron microscope. For quantitation, the widths of 10 fibers within an image for a total of 10 images per sample ($n = 3$ per treatment) were determined using ImageJ.[27]

Fibroblast proliferation

Scaffolds were immobilized onto glass coverslips (G420-15; ProSciTech) using medical-grade RTV silicone adhesive. All samples were disinfected in 70% ethanol for 30 min and washed five times with PBS. For proliferation assays, HDF (10,000 cells per well, passage 18) were plated in 24-well plates for 3 and 5 days. Proliferation of cells on hybrid and tropoelastin scaffolds was analyzed in comparison to E2A. Cells were quantified at 3 and 5 days postseeding using the MTT (3-[4,5-dimethylthiazol-2-yl]-2,5 diphenyltetrazolium bromide) assay.

Mechanical testing

Crosslinked, PBS-hydrated samples (dimensions 3×1 cm, dog-bone shape) were subjected to increasing vertical force using an Instron 5543 testing machine in uniaxial tension with a 1 kN load cell at a constant strain rate of 2 mm/min until failure.[28] The length, width, and thickness of each sample ($n = 3$ per condition) were measured using digital calipers before each test. Ultimate tensile strength was calculated based on the maximum strain at break. The calculation of stress was based on the cross-sectional area of each of the samples. Young's modulus was calculated as the slope of the stress–strain curve generated over the linear portion of the strain range after the initial toe region.[25]

Swelling

Preweighed scaffolds ($n = 3$ per condition) were submerged in Milli-Q water (Millipore) for 24 h at 37°C. Excess water was drained and the scaffolds were weighed to give the tared weight, which yielded the amount of water absorbed per gram of scaffold.

Microcomputed tomography

Scaffolds ($n = 2$ per condition) were scanned with a Sky-Scan 1072 microcomputed tomography (micro-CT) system using a 60 kV X-ray beam at a resolution of 3.5 μm. The X-ray

projection images were converted into a stack of cross sections with the NRecon 1.4.4 cone-beam reconstruction program (SkyScan) and rendered into a three-dimensional structure with VGStudio Max 1.2.1 (Volume Graphics GmbH). Scaffold porosity was estimated from the cross-section images using CTan software (SkyScan).[29]

Mouse subcutaneous implantation

Study approval was obtained from the University of Sydney Animal Ethics Committee (protocol number K20/12-2011/3/5634). Experiments were conducted in accordance with the Australian Code of Practice for the Care and Use of Animals for Scientific Purpose. Control E2A (1 mL/h), control tropoelastin-only (1 mL/h), or E2A/tropoelastin hybrid discs (1 or 3 mL/h, 4-mm-diameter circles) were disinfected in 70% ethanol and stored in PBS at room temperature before subcutaneous implantation. Thirty-two age-matched, 8-week-old male mice (C57B/l6) were purchased from Laboratory Animal Service (NSW, Australia). The dorsal surface of each mouse was shaved and cleaned with Betadine solution and then sterile saline after anesthesia. Four 1.5 cm incisions (two rows side by side) were then cut through the skin to create four subcutaneous pockets and an implant was inserted into each incision.[30] Control tropoelastin-only discs (1 mL/h) were not robust enough to be successfully implanted in all mice. The wounds were closed with 6-0 silk sutures. After the implantation, each mouse was caged individually with water and food. Mice ($n=8$) were euthanized on days 1, 7, 14, and 28 postimplantation. Skin biopsies were immediately fixed and embedded in paraffin as previously described.[30] Tissue samples were cut into 5-μm-thick transverse sections using a rotary microtome, deparaffinized, and stained using standard hematoxylin–eosin staining to assess total capsule cellularity and scaffold cell infiltration.[31]

Image analysis

Image analysis was used to perform quantitation for histopathological analyses, as previously described.[30] Briefly, 20 fields per sample were captured and images were analyzed using ImagePro Plus 7 (Media Cybernetics). Positive staining areas, defined by selecting pixels of interest, were expressed relative to the total area of the tissue of interest within the image. The cell counting macro within ImagePro Plus 7 was used to determine the number of cells per area, and identified areas were manually verified to correct for clustered cell groups.

Statistical analysis

Data are expressed as mean ± standard error of mean and statistical significance indicated in figures as $*p<0.05$, $**p<0.01$, and $***p<0.001$. The data were compared using ANOVA followed by Bonferroni's *post-hoc* test using GraphPad Prism Mac v5.00 (GraphPad Software).

Results

Electrospun E2A materials

The optimal concentration of E2A for electrospinning was determined by measuring the percentage of collector coverage following delivery of a defined amount of solution (Fig. 1A). Generally, collector coverage increased with E2A concentration, with some effect from flow rate at concentrations less than 8% w/v. The highest coverage at all flow rates tested was seen for 10% w/v E2A, with 91.6% ± 0.3%, 96.3% ± 1.4%, and 96.6% ± 0.8%, respectively, for 1, 3, and 5 mL/h conditions. The average fiber diameter at the fixed flow rate of 1 mL/h was also influenced by the solution concentration, increasing from 0.67 ± 0.02 μm at 5% w/v to a high of 1.38 ± 0.01 μm for 8% w/v (Fig. 1B). The average fiber diameters for 9% and 10% w/v were 0.96 ± 0.02 and 1.03 ± 0.03 μm, not significantly different from each other.

The distance from the electrospinning tip to the sample collector had no effect on the 10% w/v E2A fiber diameter (Fig. 1C). In contrast, increasing the flow rate from 1 to 3 mL/h significantly raised the average fiber diameter from 1.03 ± 0.02 to 2.02 ± 0.02 μm (Fig. 1D, $p<0.001$). A further significant increase was observed for a flow rate of 5 mL/h, to 2.41 ± 0.03 μm ($p<0.001$), relative to both 1 and 3 mL/h. Representative SEM images show predominantly flat, ribbon-like fibers, especially at higher flow rates (Fig. 2E).

Electrospun polyurethane/tropoelastin hybrid materials

E2A was optimally blended with tropoelastin in a 1:2 ratio by weight to generate hybrid electrospun fibers, explicitly when 100 mg of E2A was combined with 200 mg tropoelastin per mL of solution (100:200 mg/mL). A range of other ratios with lower overall protein amounts failed to maintain sufficient solution viscosity to produce electrospun fibers. Only at very high E2A concentrations (>300 mg/mL) and low tropoelastin ratios (e.g., 320:32, 350:20, and 300:20 mg/mL) were fibers produced. Resulting scaffolds had very low ultimate tensile strength and corresponding poor handling characteristics (Supplementary Fig. S1; Supplementary Data are available online at www.liebertpub.com/tea).

In the absence of crosslinking, 1:2 ratio hybrid scaffolds diminished following immersion in PBS (Fig. 2A). This was solved by crosslinking with GA before wetting, which then promoted the retention of scaffold size and shape. Following GA stabilization, hybrid fibers spun at 1 mL/h displayed an average width of 0.64 ± 0.01 μm, which increased to 1.12 ± 0.04 μm at 3 mL/h ($p<0.001$, Fig. 2B). A further increase to 1.50 ± 0.06 μm ($p<0.001$) was observed at a flow rate of 5 mL/h. With increasing flow rate, there was also a trend to greater fiber variability within a sample, with maximum fiber widths increasing from 1.01 to 2.96 and 6.01 μm for 1, 3, and 5 mL/h, respectively. Representative SEM images demonstrate the variability seen with higher flow rates (Fig. 2C). Hybrid scaffolds electrospun at 5 mL/h lacked mechanical integrity and were difficult to handle and characterize thoroughly. Accordingly, only 1 and 3 mL/h hybrids were investigated further.

Tropoelastin enhances fibroblast proliferation

The proliferation of HDF on E2A, hybrid, and all tropoelastin fibers (all 1 mL/h) was compared at days 3 and 5 (Fig. 3A). On day 3, hybrid fibers supported a 105.8% ± 1.4% increase in fibroblast proliferation relative to E2A alone ($p<0.001$). All tropoelastin scaffolds showed a further 19.1% ± 0.3% increase over hybrid fibers ($p<0.01$). On day 5, proliferation on all three surfaces increased relative to day 3, demonstrating ongoing cell viability. Consistent with day 3

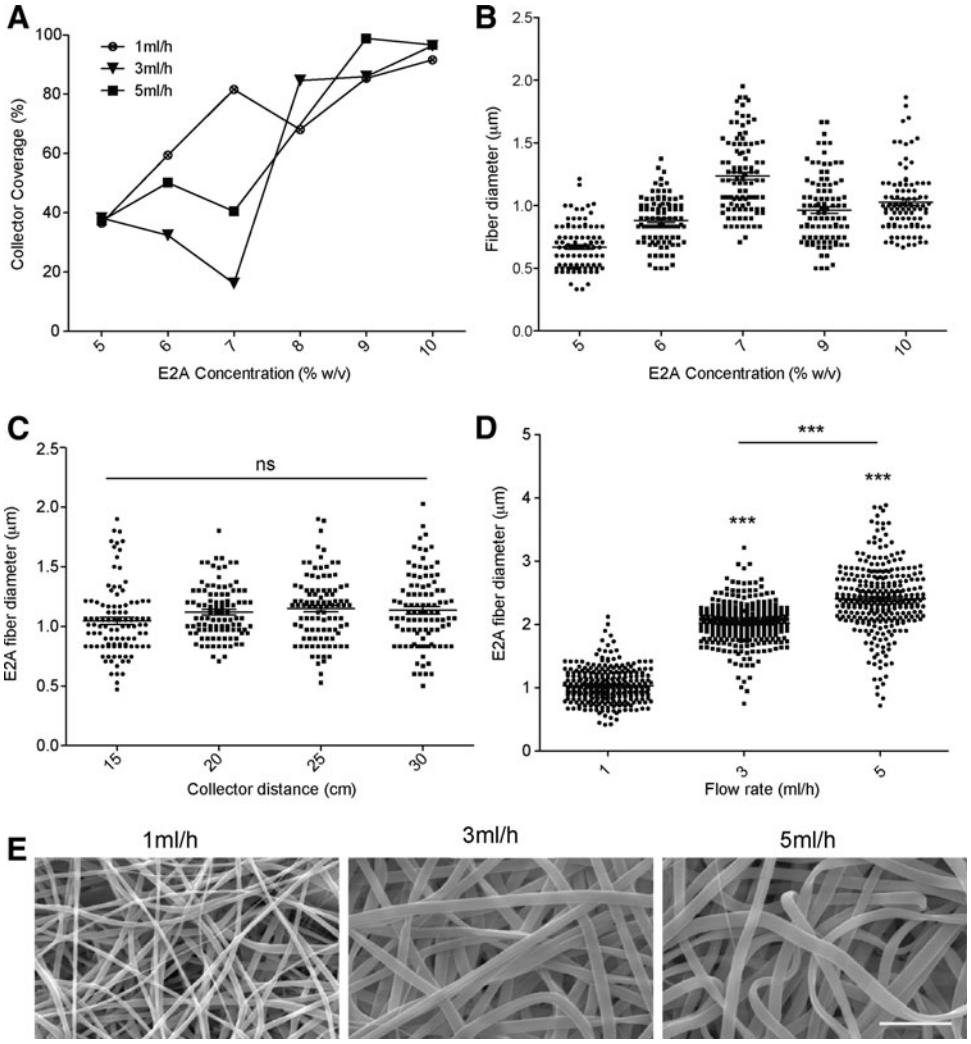

FIG. 1. Electrospinning E2A scaffolds. **(A)** Collector coverage for increasing E2A concentrations at 1 mL/h (*circles*), 3 mL/h (*triangles*), and 5 mL/h (*squares*) and **(B)** fiber diameter was not significantly changed with concentration or **(C)** collector distance. **(D)** At a fixed concentration of 10% w/v E2A, fiber diameter increased significantly from 1 to 3 mL/h and 5 mL/h (***$p < 0.001$, relative to 1 mL/h unless otherwise indicated). **(E)** Representative SEM images demonstrate this trend. Fibers at 3 and 5 mL/h have a distinct ribbon-like appearance. Scale bar = 10 μm. ns, nonsignificant; SEM, scanning electron microscopy.

trends, hybrid fibers supported a $57.4\% \pm 1.7\%$ ($p < 0.001$) increase in proliferation, while all tropoelastin scaffolds saw a further $16.7\% \pm 0.3\%$ ($p < 0.01$) increase, relative to E2A alone. Representative SEM images from day 5 show incomplete cell coverage on E2A scaffolds, but near uniform coverage of both hybrid and all tropoelastin scaffolds (Fig. 3B).

Enhanced elasticity of the hybrid

With Young's moduli of 177 ± 21 and 87 ± 12 kPa for the 1 and 3 mL/h, respectively, the blends were much more elastic than E2A (1351 ± 42 kPa). Hybrids at 1 mL/h displayed an ultimate tensile strength of 533 ± 57 and 227 ± 21 kPa for 3 mL/h. In contrast to E2A, the hybrids maintained linear elasticity responses over three- to fourfold strain until break (Fig. 4A, B).

Increased flow rate increases scaffold swelling and porosity

The porosity of E2A and tropoelastin containing hybrid scaffolds was assessed with micro-CT imaging (Fig. 5A). For spinning at 1 mL/h, there was no significant difference between the porosity of E2A only ($45.7\% \pm 4.3\%$) and hybrid ($56.2\% \pm 2.2\%$) scaffolds. However, for hybrid scaffolds spun at 3 mL/h, porosity was higher ($72.1\% \pm 0.7\%$, $p < 0.01$), with a total $57.9\% \pm 5.5\%$ increase over E2A. The physical properties of electrospun E2A scaffolds were also modified by incorporation of tropoelastin. In a swelling assay, the relative mass of water absorbed was 8.2 ± 2.3 gH_2O/g scaffold for E2A alone (Fig. 5B). Hybrid scaffolds swelled to 30.8 ± 0.4, an increase of $276\% \pm 4\%$. Increasing the flow rate from 1 to 3 mL/h further increased the swelling ratio to 53.7 ± 3.9 gH_2O/g scaffold. Representative SEM images pre- and postswelling show that changes in swelling reflected permanent structural changes in hybrid scaffolds spun at either flow rate, replacing individual fibers with a hydrogel-like appearance (Fig. 5C).

Hybrid scaffolds are better tolerated in mouse subcutaneous implantation

Hematoxylin and eosin staining of mouse subcutaneous implants after 1, 7, 14, and 28 days *in vivo* revealed substantial differences in the host response of E2A compared to hybrid materials. The number of cells present in the fibrous capsule was quantified as a marker of fibrotic response and showed significant differences between samples (Fig. 6A). At each time point, E2A-only materials had the highest

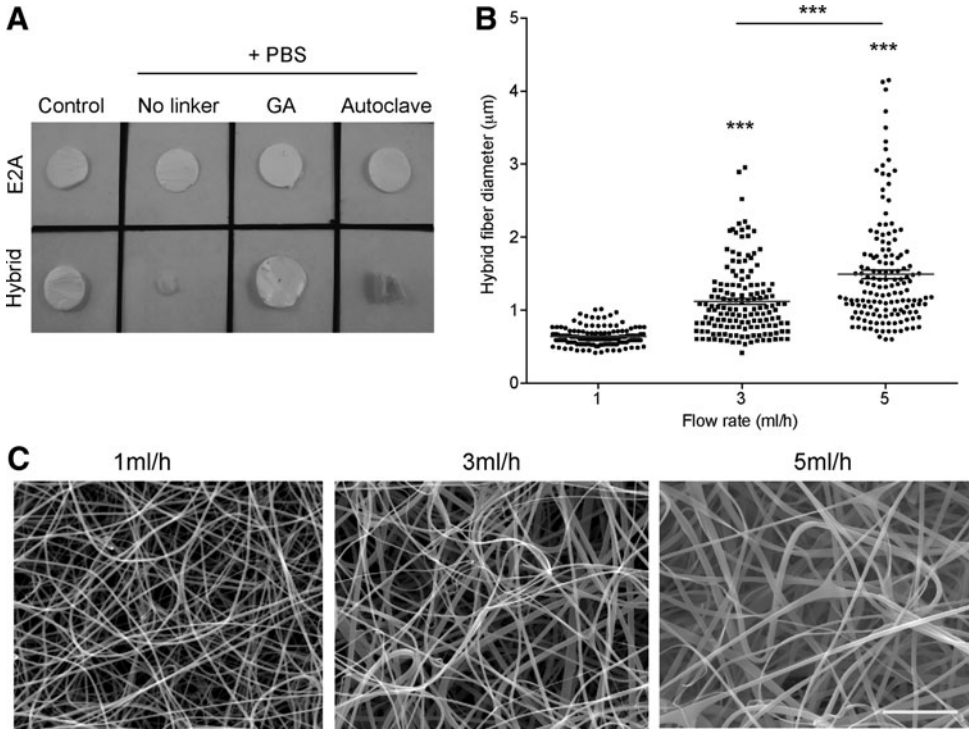

FIG. 2. Electrospinning hybrid scaffolds. **(A)** E2A and E2A/tropoelastin hybrids (1:2 w/w) when dry (control), and in the presence of phosphate-buffered saline with no crosslinking, glutaraldehyde, and following autoclaving. **(B)** Flow rate significantly increased fiber diameter (***$p < 0.001$, relative to 1 mL/h unless otherwise indicated), demonstrated in **(C)** representative SEM images. Scale bar = 10 μm.

capsule cell number, while hybrid scaffolds showed consistent reductions. By day 7, capsule cellularity was reduced by 62.6% ± 12.2% for 1 mL/h and 63.0% ± 8.9% for 3 mL/h hybrid scaffolds, relative to E2A ($p < 0.001$). These differences persisted through the study, such that by day 28, cellularity remained reduced by 68.7% ± 7.8% and 83.4% ± 9.5% for 1 and 3 mL/h hybrid scaffolds relative to E2A ($p < 0.001$). Similarly, the hybrid scaffold showed enhanced ability to promote cell ingrowth (Fig. 6B). At each time point, hybrid 3 mL/h scaffolds had the highest number of ingrowth cells, significantly greater than E2A. Hybrid scaffolds electrospun at 3 mL/h demonstrated an advantage over those electrospun at 1 mL/h. By day 7, hybrid 3 mL/h scaffolds showed enhanced cell ingrowth fourfold over E2A and twofold better than 1 mL/h hybrids. By day 28, the number of ingrowth cells in hybrid 3 mL/h scaffolds was 101.5% ± 12.6% greater than E2A and 218% ± 36% more than 1 mL/h equivalents. Representative histology images (Fig. 6C) highlight the differences in cell

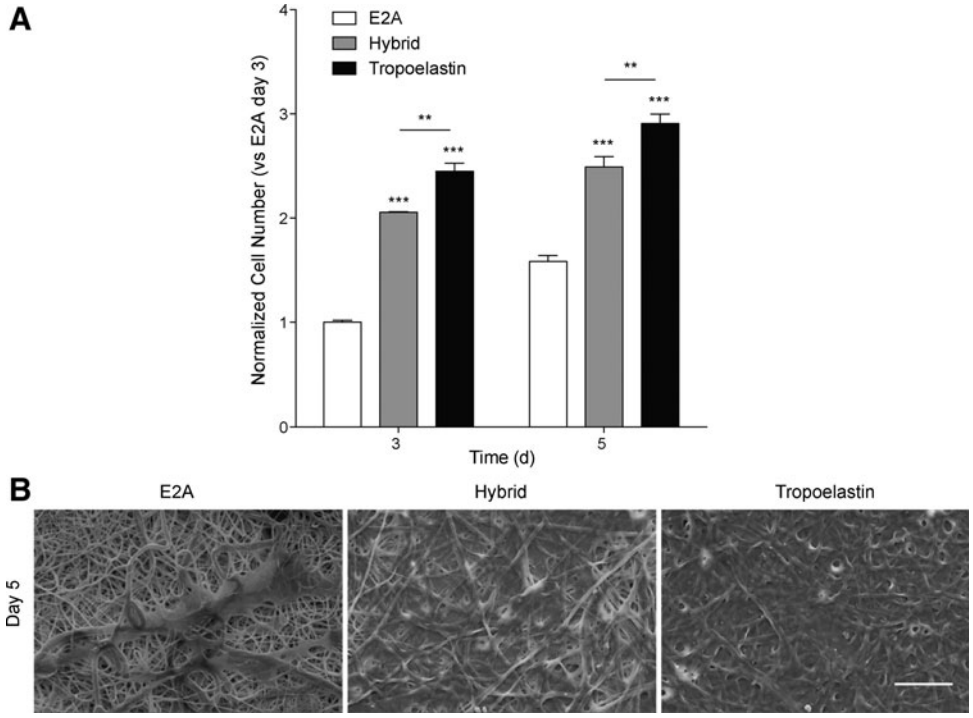

FIG. 3. **(A)** Fibroblast proliferation on E2A and hybrid scaffold at days 3 and 5. The incorporation of tropoelastin enhanced proliferation at both time points relative to E2A (**$p < 0.01$, ***$p < 0.001$, relative to E2A on each day unless otherwise indicated). **(B)** Representative SEM images show sparse cell coverage on E2A, increasing for the hybrid scaffold. Scale bar = 20 μm.

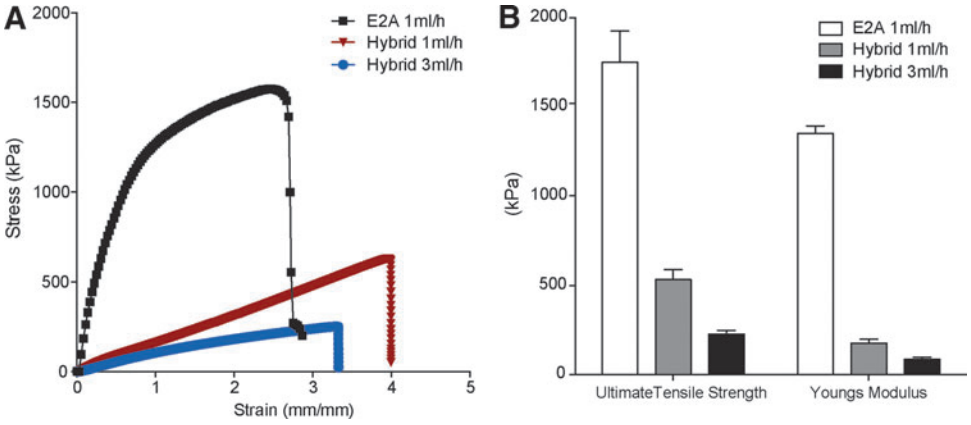

FIG. 4. **(A)** Representative stress–strain curves for E2A and hybrid scaffolds. **(B)** Ultimate tensile strength and Young's modulus calculations demonstrate that hybrid constructs had greater elasticity and reduced ultimate tensile strength than E2A. Color images available online at www.liebertpub.com/tea

numbers in the capsule (black arrows) and within the implant body (white arrows) across the 28-day time course.

Elastin content and scaffold degradation

Movat's pentachrome staining, showing elastin-rich fibers in black and collagen in yellow, also demonstrated interesting differences between the implants. The percentage area staining black in each scaffold was determined (Fig. 7A). E2A scaffolds had negligible elastin content at all time points. In contrast, both the hybrid scaffolds strongly stained for elastin fibers, consistent with the presence of tropoelastin. The increased porosity of the 3 mL/h hybrid scaffolds was reflected in a lower elastin staining area, down from 65.8% ± 7.5% to 54.5% ± 3.9% at day 1 and from 71.7% ± 3.1% to 54.9% ± 5.6% by day 7. Interestingly, the elastin content for the 1 mL/h hybrid stayed constant over the time course, while a significant drop was observed for the 3 mL/h hybrid starting at day 14 (Fig. 7B).

Discussion

Elastomers with silicone-containing chain extenders, including Elast-Eon have been developed to be soft elastic polyurethanes with exceptional biostability. However, in many cases, these components are inherently resistant to cell adhesion and support poor cell growth. With a clear emphasis on biostability and mechanical properties, less attention has been given to modulating the tissue integration of this class of materials. We identified tropoelastin as a potential copolymer that would

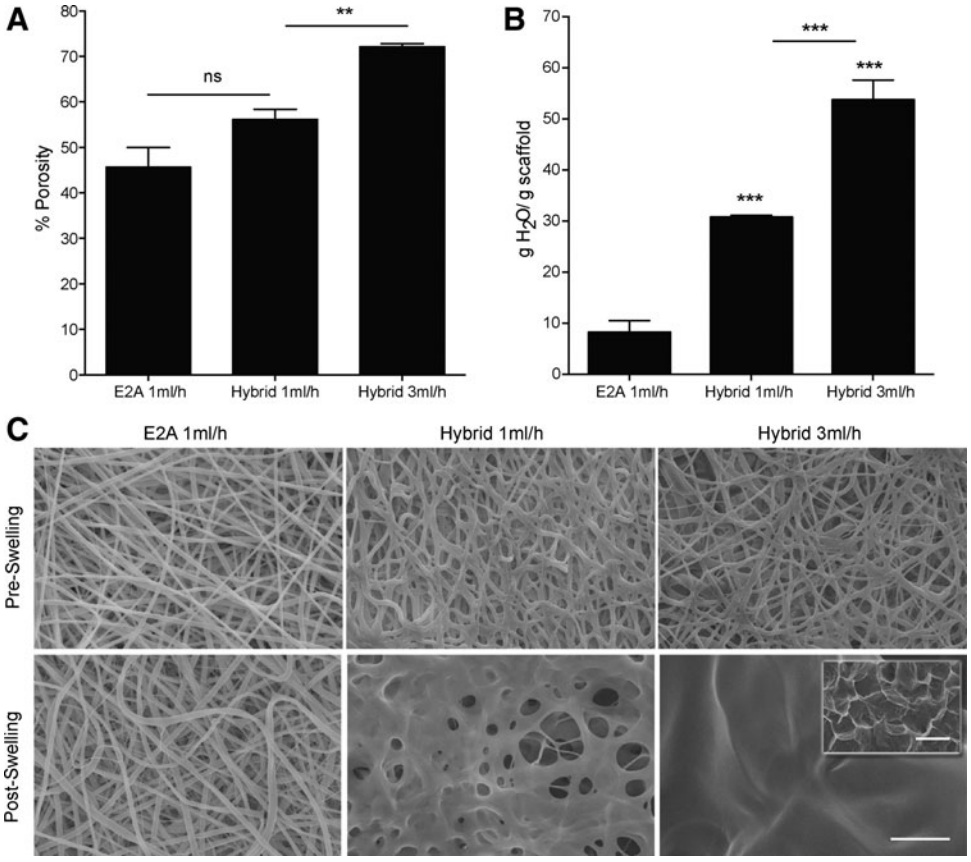

FIG. 5. **(A)** Scaffold porosity measured using microcomputed tomography. Hybrid scaffolds produced at 1 mL/h trend toward an increased porosity but were not significantly different from E2A. However, 3 mL/h hybrid scaffolds were significantly more porous (**$p < 0.01$). **(B)** Water absorption relative to scaffold weight demonstrates significantly increased swelling for both tropoelastin containing hybrids (***$p < 0.001$, relative to 1 mL/h unless otherwise indicated). **(C)** Representative SEM images show scaffold structure before and after swelling. The fibrous E2A-only architecture was unchanged, while tropoelastin containing hybrids became more gel like postswelling. *Inset* shows a honeycomb-like structure characteristic of elastin-based hydrogels and natural elastin. Scale bars = 20 μm and 200 μm for *inset*.

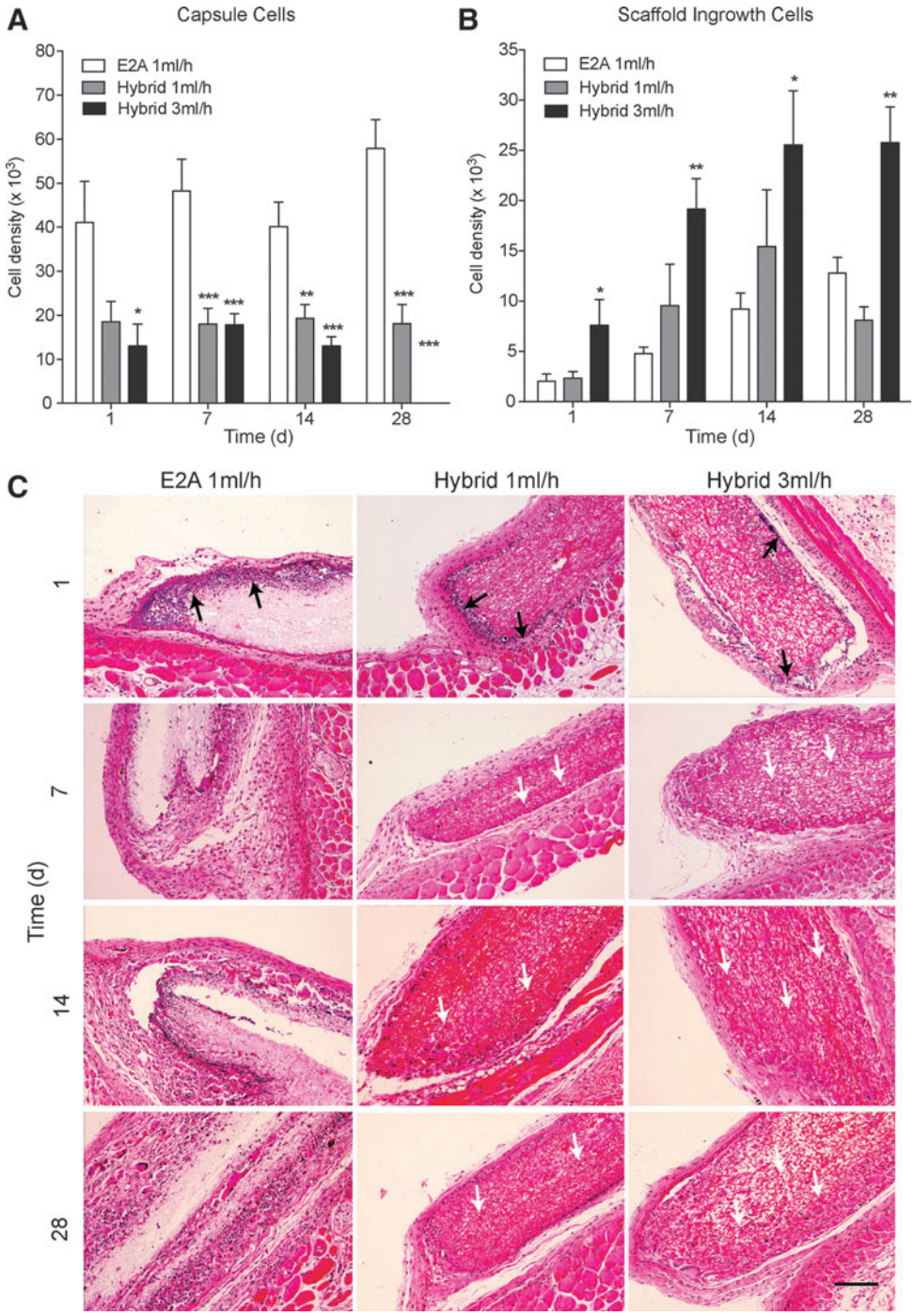

FIG. 6. Hematoxylin–eosin staining of mouse subcutaneous implants. Quantification of total cell numbers in **(A)** the implant capsule and **(B)** infiltrating into the scaffolds. Hybrid scaffold had significantly less capsule cellularity and a combination of increased porosity and tropoelastin incorporation led to significantly greater cell infiltration (statistics relative to E2A at each time point) $*p<0.05$, $**p<0.01$, $***p<0.001$. **(C)** Representative images from 1, 7, 14, and 28 days highlight differences in capsule cells (*black arrows*) and those infiltrating the scaffolds (*white arrows*). Scale bar = 200 µm. Color images available online at www.liebertpub.com/tea

enhance the overall bioactivity of Elast-Eon while maintaining its favorable mechanical properties. The previous use of electrospun tropoelastin alone and as a copolymer for PCL and collagen has demonstrated its utility in materials engineering for dermal[32] and vascular applications[33] in particular.

Screening of electrospinning parameters for E2A identified 100 mg/mL (10% w/v) as the optimal concentration for efficient collection coverage and control of fiber parameters, when using HFP as a solvent. Electrospinning of tropoelastin has been previously well described for solutions of 200 mg/mL in HFP.[34] Blends of E2A and tropoelastin could only be successfully electrospun in a small window of concentrations and ratios, all requiring total solution concentrations of 300 mg/mL or greater, in contrast to previous reports for other systems. Other ratios previously shown to work for PCL/tropoelastin hybrids (27:75, 50:50, and 75:25 mg/mL) resulted in solutions with viscosity too low to produce electrospun fibers.[24] The disruption of viscosity of a 100 mg/mL solution of E2A and tensile strength of electrospun fibers by the addition of tropoelastin at any concentration below 200 mg/mL suggests that the protein influenced interactions between E2A chains. Consistent with our previous findings for PCL/tropoelastin and collagen/tropoelastin systems, GA vapor crosslinking preserved scaffold integrity,[21] and increasing flow rates led to

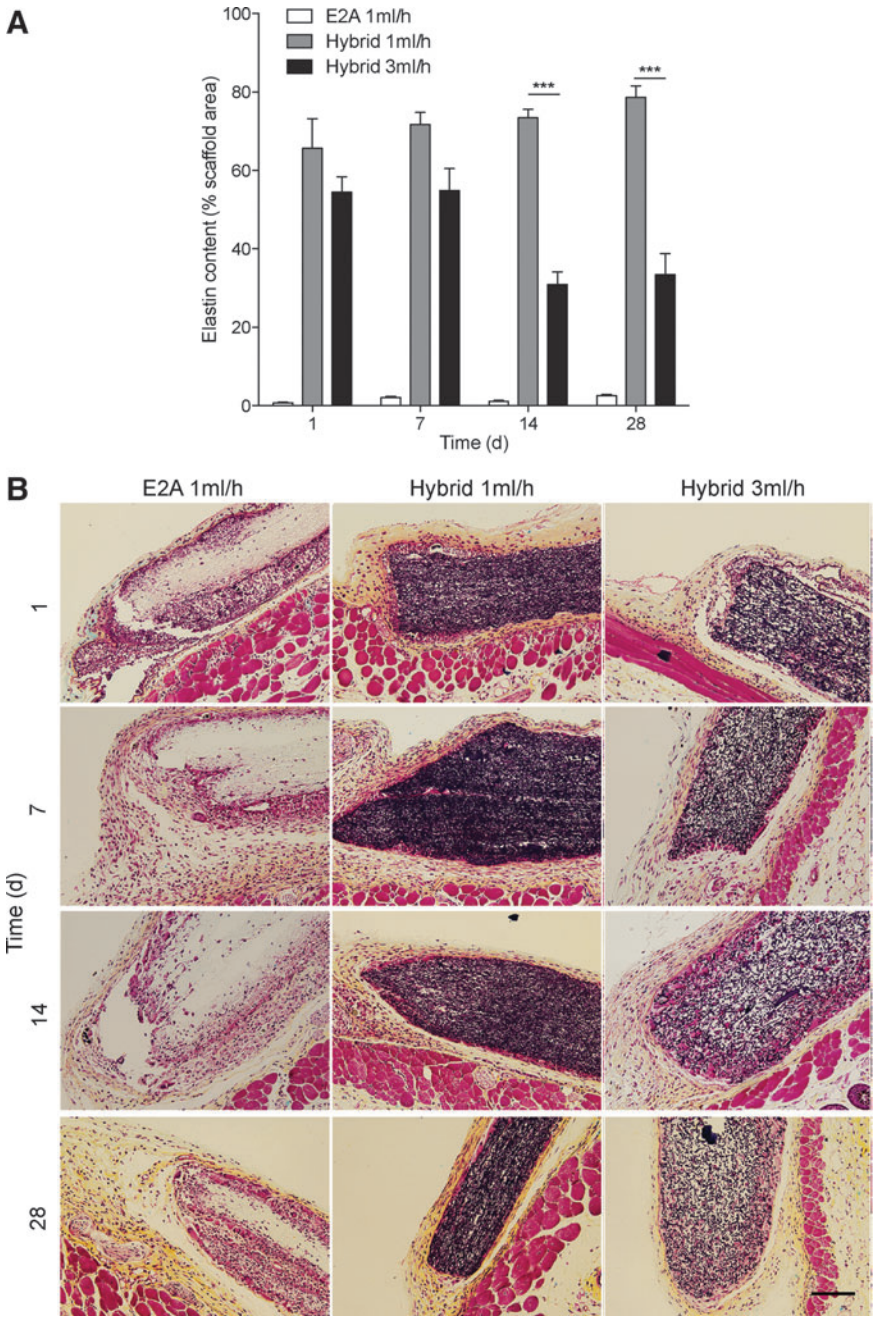

FIG. 7. Movat's pentachrome staining of mouse subcutaneous implants. **(A)** Quantification of total elastin content showed that 1 mL/h hybrid scaffolds remained stable, while the 3 mL/h equivalent degraded from 14 days. ***$p < 0.001$. **(B)** Representative images show elastin staining *black*, collagen *yellow*, and muscle *red*. Scale bar = 200 μm. Color images available online at www.liebertpub.com/tea

higher fiber diameters and corresponding gains in porosity.[20] This relationship of flow rate and porosity has been previously described.[35]

Fibroblasts are known to bind tropoelastin with high affinity, utilizing at least two major integrin binding sites.[36,37] Fibroblasts also actively migrate into electrospun tropoelastin scaffolds designed for dermal applications, depositing increasing amounts of collagen type I and fibronectin over time.[20] Hybrid E2A/tropoelastin fibers were more favorable for fibroblast growth than E2A alone, but not equivalent to all tropoelastin fibers, suggesting that many, but not all cell binding motifs, remained accessible in the hybrid. Given that tropoelastin is also known to interact strongly with endothelial cells when used as a surface coating,[38] or when electrospun into fibers,[24] it is reasonable to expect that E2A/tropoelastin hybrids would behave similarly, but this will be verified in future work.

Electrospun tropoelastin-alone scaffolds have been characterized previously. These scaffolds are elastic (Young modulus 140–220 kPa), but have modest ultimate tensile strength (150–220 kPa).[20] In combination with PCL, tensile strength can be increased up to 1950 kPa, while largely retaining the elastic properties of tropoelastin (Young modulus 310 kPa).[24] The stiffness of tropoelastin containing scaffold can be significantly increased by the inclusion of >50% w/v collagen (Young's modulus 840 kPa). In this context, the current E2A/tropoelastin system delivers a unique combination of high mechanical strength (up to 533 kPa) and low elastic modulus (87–177 kPa), modulated, in part, by scaffold fiber diameter. The porosity of hybrid scaffolds was

dominantly increased by electrospinning flow rate, leading to larger fiber diameters, consistent with previous literature.[39] Swelling increased initially with incorporation of tropoelastin and then further with increased flow rate, leading to post-swelling structures reminiscent of tropoelastin hydrogels.[40] Together, the presence of tropoelastin and the modulation of flow rate allow for the tuning of mechanical properties and swelling behavior leading to scaffolds that are expected to behave very differently *in vivo*.

In a mouse subcutaneous implant model, we observed substantial differences in the biological response to E2A and hybrid scaffolds. All tropoelastin electrospun scaffolds have previously been assessed *in vivo* as topical dermal replacements, but did not have sufficient mechanical strength to be successfully delivered to a subcutaneous pocket, excluding them from comparative study. E2A displayed the highest number of capsule infiltrating cells, but the lowest number subsequently growing into the scaffold. The high cellularity of the capsule surrounding the E2A implants is suggestive of a greater immune response. Previous research similarly demonstrated a high level of capsule cellularity for Elast-Eon-only implants, which was suppressed when the material was loaded with dexamethasone.[6] The inclusion of tropoelastin has also been shown to reduce the capsule thickness and cellularity of silk-based biomaterials, providing evidence of tropoelastin modulating implant immune response.[30] Further analysis of the cell types present in the capsule is required to draw definitive conclusions.

Changes in cell ingrowth are driven, in part, by greater scaffold porosity, but the largest improvements were seen for 3 mL/h hybrids, which combine increased porosity with cell signaling motifs found on tropoelastin. Higher scaffold ingrowth is correlated to improved biocompatibility and is a necessary precursor to positive remodeling events.[41] Evidence of scaffold remodeling was observed by tracking elastin content over time. Cellular ingrowth correlated with reduced elastin content over 28 days in high-porosity (3 mL/h) hybrid scaffolds, while 1 mL/h hybrids showed 3.2-fold less cell infiltration at 28 days and elastin remained stable. While elastin staining dominantly recognized tropoelastin present in the scaffolds, we cannot exclude the less likely possibility of *in vivo* elastogenesis.

We conclude that blending with tropoelastin improves the *in vitro* cell compatibility of E2A scaffolds and modifies the physical characteristics of the material. With their greater capacity for swelling and with higher flow rates, higher porosity, hybrid scaffolds were better tolerated in a subcutaneous mouse implant model. The altered remodeling profile of hybrid scaffolds depended on the electrospinning flow rate and provided a mechanism to tailor E2A/tropoelastin hybrid materials and so influences cell infiltration and scaffold degradation while maintaining a favorably reduced fibrotic response. This system has the potential for development of new materials suited to dermal repair and vascular grafting, where tunable mechanical properties and bioactivity of tropoelastin would provide clear benefits.

Acknowledgments

The authors acknowledge funding from the Australian Research Council (M.M.M.B., A.S.W., and S.B.) and National Institutes of Health (EB014283; A.S.W.). A.S.W. is the Scientific Founder of Elastagen Pty Ltd. They also acknowledge a postgraduate scholarship from The Sydney Medical School, University of Sydney (H.L.). The authors declare no conflict of interest in this work. They also acknowledge the facilities as well as scientific and technical assistance at the Australian Centre for Microscopy and Microanalysis.

Disclosure Statement

No competing financial interests exist.

References

1. Gunatillake, P.A., Meijs, G.F., McCarthy, S.J., and Adhikari, R. Poly(dimethylsiloxane)/poly(hexamethylene oxide) mixed macrodiol based polyurethane elastomers. 1. synthesis and properties. J Appl Poly Sci **76,** 2026, 2000.
2. Gunatillake, P.A., Martin, D.J., Meijs, G.F., McCarthy, S.J., and Adhikari, R. Designing biostable polyurethane elastomers for biomedical implants. Aust J Chem **56,** 545, 2003.
3. Santerre, J.P., Woodhouse, K., Laroche, G., and Labow, R.S. Understanding the biodegradation of polyurethanes: from classical implants to tissue engineering materials. Biomaterials **26,** 7457, 2005.
4. Simmons, A., Hyvarinen, J., Odell, R.A., Martin, D.J., Gunatillake, P.A., Noble, K.R., and Poole-Warren, L.A. Long-term in vivo biostability of poly(dimethylsiloxane)/poly(hexamethylene oxide) mixed macrodiol-based polyurethane elastomers. Biomaterials **25,** 4887, 2004.
5. Bernacca, G.M., O'Connor, B., Williams, D.F., and Wheatley, D.J. Hydrodynamic function of polyurethane prosthetic heart valves: influences of Young's modulus and leaflet thickness. Biomaterials **23,** 45, 2002.
6. Simmons, A., Padsalgikar, A.D., Ferris, L.M., and Poole-Warren, L.A. Biostability and biological performance of a PDMS-based polyurethane for controlled drug release. Biomaterials **29,** 2987, 2008.
7. Padsalgikar, A., Cosgriff-Hernandez, E., Gallagher, G., Touchet, T., Iacob, C., Mellin, L., Norlin-Weissenrieder, A., and Runt, J. Limitations of predicting in vivo biostability of multiphase polyurethane elastomers using temperature-accelerated degradation testing. J Biomed Mater Res B Appl Biomater **103,** 159, 2015.
8. Stefanovic, I.S., Djonlagic, J., Tovilovic, G., Nestorov, J., Antic, V.V., Ostojic, S., and Pergal, M.V. Poly(urethane-dimethylsiloxane) copolymers displaying a range of soft segment contents, noncytotoxic chemistry, and nonadherent properties toward endothelial cells. J Biomed Mater Res A **103,** 1459, 2015.
9. Bax, D.V., Kondyurin, A., Waterhouse, A., McKenzie, D.R., Weiss, A.S., and Bilek, M.M. Surface plasma modification and tropoelastin coating of a polyurethane co-polymer for enhanced cell attachment and reduced thrombogenicity. Biomaterials **35,** 6797, 2014.
10. Sridhar, R., Lakshminarayanan, R., Madhaiyan, K., Amutha Barathi, V., Lim, K.H., and Ramakrishna, S. Electrosprayed nanoparticles and electrospun nanofibers based on natural materials: applications in tissue regeneration, drug delivery and pharmaceuticals. Chem Soc Rev **44,** 790, 2015.
11. Klumpp, D., Rudisile, M., Kuhnle, R.I., Hess, A., Bitto, F.F., Arkudas, A., Bleiziffer, O., Boos, A.M., Kneser, U., Horch, R.E., and Beier, J.P. Three-dimensional vascularization of electrospun PCL/collagen-blend nanofibrous scaffolds in vivo. J Biomed Mater Res A **100,** 2302, 2012.

12. Lee, B.K., Ju, Y.M., Cho, J.G., Jackson, J.D., Lee, S.J., Atala, A., and Yoo, J.J. End-to-side neurorrhaphy using an electrospun PCL/collagen nerve conduit for complex peripheral motor nerve regeneration. Biomaterials **33,** 9027, 2012.
13. Ajalloueian, F., Zeiai, S., Fossum, M., and Hilborn, J.G. Constructs of electrospun PLGA, compressed collagen and minced urothelium for minimally manipulated autologous bladder tissue expansion. Biomaterials **35,** 5741, 2014.
14. Jia, L., Prabhakaran, M.P., Qin, X., and Ramakrishna, S. Guiding the orientation of smooth muscle cells on random and aligned polyurethane/collagen nanofibers. J Biomater Appl **29,** 364, 2014.
15. Detta, N., Errico, C., Dinucci, D., Puppi, D., Clarke, D.A., Reilly, G.C., and Chiellini, F. Novel electrospun polyurethane/gelatin composite meshes for vascular grafts. J Mater Sci Mater Med **21,** 1761, 2010.
16. Heo, D.N., Yang, D.H., Lee, J.B., Bae, M.S., Kim, J.H., Moon, S.H., Chun, H.J., Kim, C.H., Lim, H.N., and Kwon, I.K. Burn-wound healing effect of gelatin/polyurethane nanofiber scaffold containing silver-sulfadiazine. J Biomed Nanotechnol **9,** 511, 2013.
17. Wong, C.S., Liu, X., Xu, Z., Lin, T., and Wang, X. Elastin and collagen enhances electrospun aligned polyurethane as scaffolds for vascular graft. J Mater Sci Mater Med **24,** 1865, 2013.
18. Wise, S.G., Yeo, G.C., Hiob, M.A., Rnjak-Kovacina, J., Kaplan, D.L., Ng, M.K., and Weiss, A.S. Tropoelastin: a versatile, bioactive assembly module. Acta Biomater **10,** 1532, 2014.
19. Almine, J.F., Bax, D.V., Mithieux, S.M., Nivison-Smith, L., Rnjak, J., Waterhouse, A., Wise, S.G., and Weiss, A.S. Elastin-based materials. Chem Soc Rev **39,** 3371 2010.
20. Rnjak-Kovacina, J., Wise, S.G., Li, Z., Maitz, P.K., Young, C.J., Wang, Y., and Weiss, A.S. Tailoring the porosity and pore size of electrospun synthetic human elastin scaffolds for dermal tissue engineering. Biomaterials **32,** 6729, 2011.
21. Nivison-Smith, L., Rnjak, J., and Weiss, A.S. Synthetic human elastin microfibers: stable cross-linked tropoelastin and cell interactive constructs for tissue engineering applications. Acta Biomater **6,** 354, 2010.
22. Buttafoco, L., Kolkman, N.G., Engbers-Buijtenhuijs, P., Poot, A.A., Dijkstra, P.J., Vermes, I., and Feijen, J. Electrospinning of collagen and elastin for tissue engineering applications. Biomaterials **27,** 724, 2006.
23. Stitzel, J., Liu, J., Lee, S.J., Komura, M., Berry, J., Soker, S., Lim, G., Van Dyke, M., Czerw, R., Yoo, J.J., and Atala, A. Controlled fabrication of a biological vascular substitute. Biomaterials **27,** 1088, 2006.
24. Wise, S.G., Byrom, M.J., Waterhouse, A., Bannon, P.G., Ng, M.K., and Weiss, A.S. A multilayered synthetic human elastin/polycaprolactone hybrid vascular graft with tailored mechanical properties. Acta Biomater **7,** 295, 2011.
25. Rnjak-Kovacina, J., Wise, S.G., Li, Z., Maitz, P.K., Young, C.J., Wang, Y., and Weiss, A.S. Electrospun synthetic human elastin:collagen composite scaffolds for dermal tissue engineering. Acta Biomater **8,** 3714, 2012.
26. Yeo, G.C., Baldock, C., Wise, S.G., and Weiss, A.S. A negatively charged residue stabilizes the tropoelastin N-terminal region for elastic fiber assembly. J Biol Chem **289,** 34815, 2014.
27. Collins, T.J. ImageJ for microscopy. Biotechniques **43,** 25, 2007.
28. Wakelin, E.A., Fathi, A., Kracica, M., Yeo, G.C., Wise, S.G., Weiss, A.S., McCulloch, D.G., Dehghani, F., McKenzie, D.R., and Bilek, M.M. Mechanical properties of plasma immersion ion implanted PEEK for bioactivation of medical devices. ACS Appl Mater Interfaces **7,** 23029, 2015.
29. Yeo, G.C., Baldock, C., Tuukkanen, A., Roessle, M., Dyksterhuis, L.B., Wise, S.G., Matthews, J., Mithieux, S.M., and Weiss, A.S. Tropoelastin bridge region positions the cell-interactive C terminus and contributes to elastic fiber assembly. Proc Natl Acad Sci U S A **109,** 2878, 2012.
30. Liu, H., Wise, S.G., Rnjak-Kovacina, J., Kaplan, D.L., Bilek, M.M., Weiss, A.S., Fei, J., and Bao, S. Biocompatibility of silk-tropoelastin protein polymers. Biomaterials **35,** 5138, 2014.
31. Tavakoli, N.N., Harris, A.K., Sullivan, D.R., Hambly, B.D., and Bao, S. Interferon-gamma deficiency reduces neointimal formation in a model of endoluminal endothelial injury combined with atherogenic diet. Int J Mol Med **30,** 545, 2012.
32. Machula, H., Ensley, B., and Kellar, R. Electrospun tropoelastin for delivery of therapeutic adipose-derived stem cells to full-thickness dermal wounds. Adv Wound Care **3,** 367, 2014.
33. McKenna, K.A., Hinds, M.T., Sarao, R.C., Wu, P.C., Maslen, C.L., Glanville, R.W., Babcock, D., and Gregory, K.W. Mechanical property characterization of electrospun recombinant human tropoelastin for vascular graft biomaterials. Acta Biomater **8,** 225, 2012.
34. Li, M., Mondrinos, M.J., Gandhi, M.R., Ko, F.K., Weiss, A.S., and Lelkes, P.I. Electrospun protein fibers as matrices for tissue engineering. Biomaterials **26,** 5999, 2005.
35. Lowery, J.L., Datta, N., and Rutledge, G.C. Effect of fiber diameter, pore size and seeding method on growth of human dermal fibroblasts in electrospun poly(epsilon-caprolactone) fibrous mats. Biomaterials **31,** 491, 2010.
36. Bax, D.V., Rodgers, U.R., Bilek, M.M., and Weiss, A.S. Cell adhesion to tropoelastin is mediated via the C-terminal GRKRK motif and integrin alphaVbeta3. J Biol Chem **284,** 28616, 2009.
37. Lee, P., Bax, D.V., Bilek, M.M., and Weiss, A.S. A novel cell adhesion region in tropoelastin mediates attachment to integrin alphavbeta5. J Biol Chem **289,** 1467, 2014.
38. Waterhouse, A., Yin, Y.B., Wise, S.G., Bax, D.V., McKenzie, D.R., Bilek, M.M.M., Weiss, A.S., and Ng, M.K.C. The immobilization of recombinant human tropoelastin on metals using a plasma-activated coating to improve the biocompatibility of coronary stents. Biomaterials **31,** 8332, 2010.
39. Loh, Q.L., and Choong, C. Three-dimensional scaffolds for tissue engineering applications: role of porosity and pore size. Tissue Eng Part B Rev **19,** 485, 2013.
40. Mithieux, S.M., Rasko, J.E., and Weiss, A.S. Synthetic elastin hydrogels derived from massive elastic assemblies of self-organized human protein monomers. Biomaterials **25,** 4921, 2004.
41. Yuan, H., Zhou, Q., Li, B., Bao, M., Lou, X., and Zhang, Y. Direct printing of patterned three-dimensional ultrafine fibrous scaffolds by stable jet electrospinning for cellular ingrowth. Biofabrication **7,** 045004, 2015.

Address correspondence to:
Anthony S. Weiss, PhD
School of Molecular Bioscience
University of Sydney
Charles Perkins Centre D17
Sydney 2006
New South Wales
Australia

E-mail: tony.weiss@sydney.edu.au

Received: September 1, 2015
Accepted: February 4, 2016
Online Publication Date: March 8, 2016